

# Localization of Electronic States in III-V Semiconductor Alloys: A Comparative Study

C. Pashartis and O. Rubel\*

*Department of Materials Science and Engineering, McMaster University,  
1280 Main Street West, Hamilton, Ontario L8S 4L8, Canada*

(Received 24 December 2016; revised manuscript received 3 May 2017; published 12 June 2017)

Electronic properties of III-V semiconductor alloys are examined using first principles, with the focus on the spatial localization of electronic states. We compare localization at the band edges due to various isovalent impurities in a host GaAs, including its impact on the photoluminescence linewidths and carrier mobilities. The extremity of localization at the band edges is correlated with the ability of individual elements to change the band gap and the relative band alignment. Additionally, the formation energies of substitutional defects are calculated and linked to challenges associated with the growth and formability of alloys. A spectrally resolved inverse participation ratio is used to map localization in prospective GaAs-based materials alloyed with B, N, In, Sb, and Bi for 1.55- $\mu\text{m}$ -wavelength telecommunication lasers. This analysis is complemented by a band unfolding of the electronic structure and a discussion of the implications of localization on the optical gain and Auger losses. Correspondence with experimental data on the broadening of the photoluminescence spectrum and charge-carrier mobilities show that the localization characteristics can serve as a guideline for the engineering of semiconductor alloys.

DOI: 10.1103/PhysRevApplied.7.064011

## I. INTRODUCTION

Semiconductor alloys are widely used as an active material in a variety of optoelectronic applications, such as lasers, solar cells, light-emitting diodes (LEDs), and photodetectors [1]. For instance, dilute bismides Ga(As,Bi) [2,3], dilute nitrides (Ga,In)(N,As) [4,5], and group-III nitrides (Al,Ga,In)N [6] represent group-III-V materials that are actively studied. Mixing of semiconductors enables tuning of their optical properties, lattice parameters (epitaxial strain), and transport characteristics to a desired application. Examples include 1.55- $\mu\text{m}$  emission wavelength in the telecommunications industry, the visible spectrum for general lighting, an ultraviolet range of wavelengths for disinfecting water, and a multijunction monolithic solar cell with 1-eV absorption edge.

Properties of the solid solutions often deviate from Vegard's law; i.e., they cannot be represented as a linear interpolation between properties of the constituents. Alloying elements perturb the electronic structure of the host material, which may introduce traps that affect the optical and transport characteristics. For instance, a band-gap bowing [7] and a broadening of the photoluminescence (PL) linewidth in dilute nitride semiconductors [8], or a drastic decrease of the hole mobility in dilute bismides [9], are attributed to band tails, which originate from the spatially localized states created by isoelectronic substitutional impurities of individual N or Bi as well as their clusters in a GaAs host [10–13]. Extrinsic factors, such as nonintentional dopant impurities, native defects, and heterostructure

interfaces, also contribute to localization; however, we will examine intrinsic factors only in our study.

Localization of electronic states can detrimentally affect the performance of devices, which should be taken into account when selecting alloying elements. In the case of solar cells, high mobility is desired for the efficient transport of photogenerated carriers to electrodes. The presence of band tails leads to an inhomogeneous broadening of the gain spectrum, causing a reduction of the peak value of intensity gain (Ref. [14], p. 221). On the other hand, a wide photoluminescence linewidth can be a desired attribute in the case of ultraviolet light sources for water purification [6] or a general-purpose LED lighting [15].

Electronic-structure calculations are widely used to explore parameter space [16] and aid in quantifying the disorder introduced into a system by isoelectronic substitutional impurities. For example, GaP:N, GaAs:Bi, and GaN:As exhibit strong spatial localization of wave functions associated with impurity states near the band edges [10, 17–20]. Examination of a three-dimensional charge-density distribution associated with an electronic state in an alloy provides some information about the extent of localization, but it lacks a quantitative criterion that distinguishes between localized and delocalized states.

Bellaiche *et al.* [17] originally proposed a localization parameter as a sum of probabilities  $\rho_\alpha(E_i)$  for finding an electron in a specific eigenstate  $E_i$  in the vicinity of atomic sites  $\alpha$  of the same element type. Deng *et al.* [21] adapted this approach to a single impurity, e.g., GaAs:X, and defined a localization ratio as the ratio of the wave-function probability amplitude at the impurity site  $X$  relative to the element it is substituted for in the host lattice,

\*rubelo@mcmaster.ca

$$\zeta = \frac{\rho_X}{\rho_{\text{Ga or As}}} - 1. \quad (1)$$

The stronger the localization is, the higher the ratio; the ratio of zero corresponds to no spatial perturbations of the electronic state. The magnitude of the ratio can be used to assess the relative impact of various impurities on the band edges of the host. However, a generalization of this approach to an *arbitrary* state in an alloy is not straightforward due to the lack of a “reference” state.

Localization in alloys can be defined as a vanishing zero-temperature dc conductivity in the system (the absence of diffusion in the Anderson model [22]). The value of conductivity as a function of the Fermi energy provides a spectral measure of localization. However, its calculation from first principles is a cumbersome process. Instead, Wegner [23] suggested the second moment of the wave-function probability amplitude, i.e., the inverse participation ratio (IPR)

$$\chi(E_i) = \frac{\int |\psi_i(\mathbf{r})|^4 d\mathbf{r}}{[\int |\psi_i(\mathbf{r})|^2 d\mathbf{r}]^2}, \quad (2)$$

as a criterion to distinguish between localized and extended states. The inverse value  $\chi^{-1}$  represents a volume within which the wave function  $\psi_i(\mathbf{r})$  is confined. It can also be related to the probability of an electron to return to the same state after an infinite time interval [24] and thus is ultimately linked to the transport properties.

Here, we use both the localization ratio and the IPR criteria to perform a comparative study of localization effects in group-III-V semiconductor alloys. First, we characterize isovalent impurities of B, N, Al, P, In, Sb, Tl, and Bi in the host GaAs. We show that the localization strength of these impurities is governed by their Born effective charges. The strength of localization also determines the ability of alloying elements to change the band gap and the relative alignment of the conduction- and valence-band edges (the CBEs and VBEs), which is important for band-gap engineering. Additionally, formation enthalpies of the individual impurities are calculated and linked to challenges associated with the growth of corresponding alloys. Finally, we compare disorder characteristics of various gain-medium materials for 1.55- $\mu\text{m}$  lasers, including  $\text{Ga}_{1-x}\text{In}_x\text{As}$ , dilute  $\text{Ga}_{1-x}\text{In}_x\text{As}_{1-y-z}\text{N}_y\text{Sb}_z$ , and  $\text{GaAs}_{1-x}\text{Bi}_x$  alloys, as well as the hypothetical  $\text{Ga}_{1-x}\text{B}_x\text{As}_{1-y}\text{Bi}_y$  compound alloys. The results of the aforementioned calculations are related to established experimental trends in transport coefficients and the PL characteristics of these alloys.

## II. COMPUTATIONAL DETAILS

### A. Electronic structure of binaries, impurities, and alloys

The first-principles calculations are carried out using density-functional theory (DFT) [25] and the linear

TABLE I. Equilibrium lattice constant  $a_0$ , band gap  $E_g$  of binary compounds in the zinc-blende structure calculated with the DFT-GGA-WC-MBJ method and compared with the experimental values gathered in Refs. [30,31].

Binary compounds	DFT		Experiment	
	$a_0$ (Å)	$E_g$ (eV)	$a_0$ (Å)	$E_g$ (eV)
BAs	4.775	1.66	...	...
BBi	5.471	0.39	...	...
GaN	4.507	2.96	4.50	3.30
GaAs	5.660	1.53	5.609	1.52
GaSb	6.116	0.72	6.096	0.81
GaBi	6.368	-1.65	...	...
InN	4.995	0.66	4.98	0.78
InAs	6.091	0.52	6.058	0.42
InSb	6.526	0.17	6.479	0.24

augmented plane-wave method implemented in the WIEN2K package, version 14.2 [26]. The Brillouin zone of the binary compounds’ primitive cell is sampled using  $8 \times 8 \times 8$  Monkhorst and Pack [27] mesh. The muffin-tin radii  $R^{\text{MT}}$  were set to 1.72, 1.85, 1.90, 1.95, 2.00, 2.00, 2.10, 2.31, 2.33, and 2.33 bohr for N, B, P, Al, Ga, As, In, Sb, Tl, and Bi, respectively. The product  $R_{\text{min}}^{\text{MT}} K_{\text{max}} = 7$ , which determines the accuracy of a plane-wave expansion of the wave function, is used throughout the calculations.

The lattice constants and the band structures of the binary compounds (Table I) are calculated self-consistently using the Wu and Cohen [28] generalized-gradient approximation (GGA WC) for the exchange-correlation functional. The choice of exchange-correlation functional is based on preliminary studies of the band structure of GaAs [20]. The Tran-Blaha modified Becke-Johnson (TBMBJ) potential [29] is applied to overcome deficiency of the semilocal exchange-correlation functional and to improve the accuracy of the band gaps.

We build 128-atom  $4 \times 4 \times 4$  supercells using a two-atom primitive-cell basis instead of the conventional eight-atom cell required for calculation of the effective band structure of an alloy. The  $k$  mesh is downscaled to  $2 \times 2 \times 2$ . The GGA-WC self-consistent lattice constant of  $a_0 = 5.660$  Å is used for the host GaAs in the single-impurity studies. The list of alloys, their bond compositions, and the expectation values of the lattice parameters are provided in Table II. In the case of alloys, the lattice constant is obtained from a linear interpolation by taking into consideration the equivalent binary concentration of the bonds. The atomic positions are optimized by minimizing Hellmann-Feynman forces acting on atoms below 2 mRy/bohr. Calculations of the Bloch spectral weight for the effective band structure are performed using the FOLD2BLOCH package [32]. Born effective charges for impurities are computed using a BERRYPI module [33] implemented in WIEN2K.

A localization ratio  $\zeta$  defined in Eq. (1) is used to evaluate the extent of localization at the band edges for

TABLE II. The bond statistics used to determine the lattice constant of alloys based on Vegard's law. These concentrations are determined by the number of bonds in the supercell. Deviations from a random alloy such as enhancement of a particular bond statistics due to short-range correlations are marked in parentheses. The sum of the concentrations adds up to 1.

Supercell composition	Equivalent binary concentration $c_i$									$a = \sum_i c_i a_0(i)$ (Å)
	BAs	BBi	GaN	GaAs	GaSb	GaBi	InN	InAs	InSb	
$\text{In}_{34}\text{Ga}_{30}\text{As}_{64}$				0.469				0.531		5.89
$\text{Ga}_{38}\text{In}_{26}\text{As}_{60}\text{N}_2\text{Sb}_2$ (In-N correlated)				0.574	0.020		0.031	0.363	0.012	5.81
$\text{Ga}_{64}\text{As}_{57}\text{Bi}_7$				0.891		0.109				5.74
$\text{Ga}_{58}\text{B}_6\text{As}_{57}\text{Bi}_7$ (B-Bi correlated)	0.057	0.036		0.832		0.075				5.65

single impurities. An arithmetic averaging of  $\zeta$ 's is performed to account for degeneracies at the band edges. We find the results to be sensitive to the size of the supercell. For instance, Deng *et al.* [21] report  $\zeta = 3.5$  at the valence-band edge for a 64-atom GaAs:Bi supercell, which can be compared to our result of  $\zeta = 5.1$  for a 128-atom supercell but differs from the value of  $\zeta = 16$ , which is obtained under identical conditions for a 432-atom supercell. Here, we constrain the size of a supercell to 128 atoms, which implies that the localization ratio may not be fully converged with respect to cell size. Nevertheless, chemical trends in a relative localization ratio  $\zeta$  computed for various impurities should be valid.

The IPR  $\chi$  is used as a measure of localization in alloys. It is evaluated on the basis of probabilities of finding an electron with an eigenenergy  $E_i$  within the muffin-tin spheres centered at atomic sites. The atomic sites,  $\alpha$ , and, correspondingly, the IPR values are split into two sublattices: groups III and V. The IPR is evaluated for each sublattice using a discrete version [34] of Eq. (2),

$$\chi^{\text{III/V}}(E_i) = \frac{\sum_{\alpha} \rho_{\alpha}^2(E_i)}{[\sum_{\alpha} \rho_{\alpha}(E_i)]^2}. \quad (3)$$

The summation index  $\alpha$  runs over all atomic sites on the group-III or -V sublattice. Here, the participation ratio  $\chi^{-1}$  represents a number of atomic sites which confine the wave function  $\psi_i(\mathbf{r})$ . The lower limit of the IPR is the inverse number of atoms in the sublattice that corresponds to the pure Bloch states. The spectrally resolved IPR is determined as a weighted average

$$\chi(E_i) = \frac{\chi^{\text{III}} w^{\text{III}} + \chi^{\text{V}} w^{\text{V}}}{w^{\text{III}} + w^{\text{V}}}, \quad (4)$$

where  $w = \sum_{\alpha} \rho_{\alpha}(E_i)$  is the eigenstate-specific weight calculated for each group of atoms. It should be noted that the muffin-tin spheres capture only a portion of the wave function (50% or less in typical calculations reported here). The remaining part of the wave function is assigned to the interstitial region and is not accounted for in the  $\rho_{\alpha}$  values.

The IPR is less sensitive to the size of the supercell, in contrast to the localization ratio. We obtain  $\chi = 0.027$  for the VBE of a 128-atom GaAs:Bi supercell vs  $\chi = 0.016$  in the reference 128-atom supercell of GaAs. In the case of a 432-atom supercell, the corresponding values are  $\chi = 0.0095$  and  $0.0046$ . In both cases the IPR increases by approximately a factor of 2 due to the disorder associated with the impurity.

## B. Defect formation energy

The formation energy of isoelectronic neutral defects is calculated using the expression [35]

$$E^f[\underline{\text{GaAs}}:X] = E_{\text{tot}}[\underline{\text{GaAs}}:X] - E_{\text{tot}}[\text{GaAs}] - \mu[X] + \mu[\text{Ga}], \quad (5)$$

where  $E_{\text{tot}}$  is the DFT total energy and  $\mu$  represents the chemical potential. The notation  $\underline{\text{GaAs}}:X$  implies that the element  $X$  is substituted in place of a Ga atom in GaAs. In the calculations, the impurity is placed in a host 128-atom  $4 \times 4 \times 4$  supercell, followed by relaxation of atomic positions while keeping the size of the cell constrained at the equilibrium value for GaAs.

Here, we assume a bulk source of impurities for B, Al, P, In, Sb, Tl, and Bi. The DFT total energy serves as an approximation for their chemical potential,

$$\mu[X] \approx E_{\text{tot}}[X_{\text{bulk}}]. \quad (6)$$

The nitrogen source is a  $\text{N}_2$  molecule, with the chemical potential approximated by

$$\mu[\text{N}] \approx \frac{1}{2} E_{\text{tot}}[\text{N}_2]. \quad (7)$$

By using DFT total energies for the chemical potential, we neglect the zero-point energy, the vibrational energy, and entropy, as well as the pressure contributions to the free energy. The chemical potential of Ga is considered within the uncertainty

$$E_{\text{tot}}[\text{GaAs}] - E_{\text{tot}}[\text{As}_{\text{bulk}}] < \mu[\text{Ga}] < E_{\text{tot}}[\text{Ga}_{\text{bulk}}], \quad (8)$$

which corresponds to Ga-poor and Ga-rich growth conditions (the lower and upper bounds, respectively). The energy width of the range is determined by the formation enthalpy of the host lattice,

$$\Delta H_f[\text{GaAs}] \approx E_{\text{tot}}[\text{GaAs}] - E_{\text{tot}}[\text{As}_{\text{bulk}}] - E_{\text{tot}}[\text{Ga}_{\text{bulk}}]. \quad (9)$$

We can rewrite Eq. (8) using the formation enthalpy as

$$E_{\text{tot}}[\text{Ga}_{\text{bulk}}] + \Delta H_f[\text{GaAs}] < \mu[\text{Ga}] < E_{\text{tot}}[\text{Ga}_{\text{bulk}}]. \quad (10)$$

It is straightforward to modify Eqs. (6)–(10) for the case of group-V-type defects,  $\text{GaAs}:X$ .

The DFT total energies are obtained using the Vienna *ab initio* simulation program and projector augmented-wave potentials [36–38]. The Perdew-Burke-Ernzerhof (PBE) generalized-gradient approximation [39] for the exchange-correlation functional is utilized to maximize the chemical accuracy of the calculations. The cutoff energy for a plane-wave expansion is set at the level of 25% higher than the value recommended in pseudopotential files (215–500 eV, depending on the chemical composition). Our calculations yield the formation enthalpy of  $\Delta H_f = -0.65$  eV per formula unit of GaAs. This result agrees reasonably well with the experimental value of  $-0.74$  eV [40], giving the uncertainty of  $\pm 0.03$  eV/atom for reaction energies obtained with DFT PBE [41].

### C. Special quasirandom alloys

The compound alloys are modeled as random unless otherwise specified in the text. Since there are multiple possible realizations of a random alloy structure, we use a special-quasirandom-structure (SQS) approach [42]. The alloy-theoretic automated toolkit package [43] is used to distribute alloying elements within the supercell of 128 atoms using the MCSQS code. The alloy state is characterized by an objective function that captures deviations of atomic correlation functions from the ideal random alloy. Our objective function includes pair, triplet, and quadruplet correlations with the cutoff distances of 8.1, 5.8, and 4.1 Å, respectively. The selection of cutoff distances corresponds to the fourth, second, and first nearest-neighbor atoms (respectively) on the same sublattice.

A metropolis Monte Carlo algorithm is utilized to minimize the objective function with a default annealing temperature. To assist the algorithm in finding a global minimum, ten differently seeded simulations are run, until convergence and the structure with the lowest objective function is chosen for the DFT calculations. Additional constraints are imposed in the SQS search algorithm to keep the supercell lattice vectors consistent with the primitive lattice and  $4 \times 4 \times 4$  multiplicity.

## III. RESULTS AND DISCUSSION

### A. Isovalent substitutional impurities in GaAs

We begin by studying localization effects caused by isolated impurities in GaAs. The aim is to identify a single characteristic that captures chemical trends and therefore can serve as a prediction tool for mixing alloy elements into a host lattice. The electronegativity is a straightforward candidate to begin with. In the case of dilute nitrides, the localization is attributed to a large electronegativity difference between N and As [17] (3.04 vs 2.18 according to Pauling’s scale [44]). On the other hand, Sb and Bi behave differently in GaAs, regardless of the nearly identical electronegativity values (2.05 vs 2.02).

The Born effective charge  $Z^*$  captures the ability of an atom to attract bonding electrons by taking into consideration the particular chemical environment. The results shown in Fig. 1 indicate that Bi in GaAs is significantly more electropositive than Sb, which translates into a greater impact of Bi on the electronic structure of GaAs. From all isovalent impurities in GaAs, nitrogen shows the most striking value of  $Z^* \approx -6$ , which is drastically different from the value of  $Z^* = -2.7$  for nitrogen in GaN [45]. The effective charge of Tl suggests that it is the most electropositive group-III element, contrary to the fact that B and Tl have identical electronegativity values [44].

Calculations of the effective charge for supercells are computationally demanding. The trend line in Fig. 1 suggests that the Born effective charge scales linearly with  $sp^3$ -hybrid orbital energies obtained from Ref. [46] (p. 50), which can be used to predict the impact of an impurity on the electronic structure of the host lattice. A significance of the relative alignment of impurity-host orbital energies for the electronic structure of alloys was previously pointed out

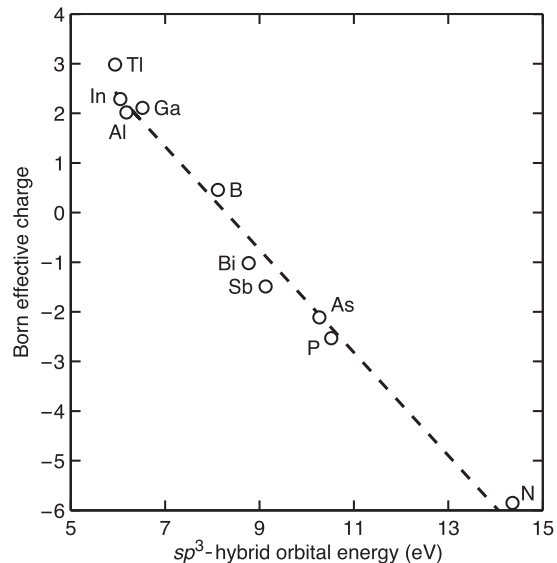


FIG. 1. Born effective charge for isovalent GaAs: $X$  impurities as a function of their  $sp^3$ -hybrid orbital energy.

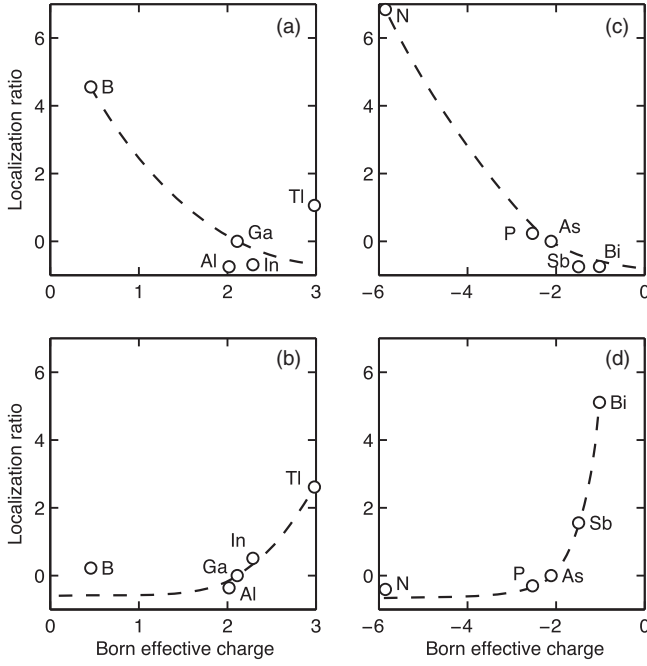


FIG. 2. Localization ratio defined by Eq. (1) for the electronic states at the (a),(c) conduction- and (b),(d) valence-band edges in GaAs due to single isovalent impurities plotted as a function of the element's Born effective charge. The dashed line is a guide for the eye.

by Deng *et al.* [21]. The orbital energies of the valence shells together with the overlap parameters are capable of capturing trap states and localization effects in various alloys, as demonstrated by O'Reilly's group from a tight-binding perspective [47,48].

Figure 2 shows the localization in CBEs and VBEs due to isovalent impurities in GaAs. Among all impurities, nitrogen introduces the strongest localization, followed by Bi and B. Those elements have more than a  $1e$  difference in the Born effective charge with respect to the host elements they are substituted for. The localization ratio due to Tl and Sb is at an intermediate level. As one would expect, elements with a lower Born effective charge are effective in capturing electrons, thus introducing localized states in the conduction band. The opposite applies to the valence band.

Signatures of the electron localization can be observed via a broadening of the low-temperature PL linewidth as well as a deterioration of the transport coefficients. The available experimental data for ternary alloys are gathered in Table III alongside the calculated values of the localization ratio. Based on these data, we can suggest a criterion of the localization ratio  $\zeta \lesssim 1$  for impurities that virtually do not impede charge-carrier transport. This guideline can be used in alloy design for applications where the charge transport plays a crucial role, e.g., photovoltaics where a high-mobility, bipolar charge-carrier transport is desired.

The ability of an individual element to change the band gap also scales with the localization ratio. Figure 3(a)

TABLE III. Localization ratio  $\zeta$  for single isovalent impurities compared to experimental values of the charge-carrier mobility  $\mu$  and the PL linewidth (the full width at half maximum).

Impurity	PL linewidth	$\mu/\mu_{\text{GaAs}}$ (%)		$\zeta$	
	(meV)	electrons	holes	CBE	VBE
GaAs (host)	5 <sup>a</sup>	100 <sup>b</sup>	100 <sup>c</sup>	0	0
GaAs:B	40,70 <sup>d</sup>	...	...	4.56	0.22
GaAs:Al	4 <sup>e</sup>	96	96 <sup>f</sup>	-0.75	-0.36
GaAs:In	2-4, 10 <sup>g</sup>	$\gtrsim 100$ <sup>h</sup>	...	-0.69	0.51
GaAs:Tl	...	...	...	1.06	2.61
GaAs:N	30, 105 <sup>i</sup>	63 <sup>j</sup>	...	6.84	-0.41
GaAs:P	10 <sup>k</sup>	$\approx 100$ <sup>l</sup>	...	0.23	-0.30
GaAs:Sb	10, 23 <sup>m</sup>	$\approx 100$	25 <sup>n</sup>	-0.75	1.55
GaAs:Bi	64, 100 <sup>o</sup>	87	18 <sup>p</sup>	-0.74	5.11

<sup>a</sup>2 K [49].

<sup>b</sup>Room temperature (Ref. [50], p. 91).

<sup>c</sup>Weakly doped room temperature [51].

<sup>d</sup>1.6% B at 300 K, pump intensity 300 W/cm<sup>2</sup>, bulklike [52], 3% B at 10 K excluding substrate [53].

<sup>e</sup>2.9% Al, 2 K, pump intensity 10<sup>-3</sup>-10 W/cm<sup>2</sup> (Ref. [54]).

<sup>f</sup>Room temperature 1.6% Al (Ref. [55], p. 626).

<sup>g</sup>Ga<sub>0.46</sub>In<sub>0.54</sub>As at 77 K [56],  $\approx 1\%$  In at 4.2 K at 10<sup>-3</sup>-10 W/cm<sup>2</sup> (Ref. [57]).

<sup>h</sup>Room temperature [58].

<sup>i</sup>Annealed structure at 5 K at 2% average of 10  $\mu$ W [59], 4 K at 1.4% [60].

<sup>j</sup>Room temperature [61].

<sup>k</sup>P 30% at 12 K quantum-well structure of  $\approx 5$  quantum wells 2.7 nm thick [57].

<sup>l</sup>Room temperature [62].

<sup>m</sup>Sb  $\approx 6\%$  at 4.2 K at (0.001-10) W/cm<sup>2</sup> (Ref. [57]), 4.4% Sb with excitation intensity of 2 W/cm<sup>2</sup> at 4 K [63].

<sup>n</sup>8% Sb, room temperature [64].

<sup>o</sup>2.6% Bi at 10 K [65], 1.3% at 9 K at 1 mW [66,67].

<sup>p</sup>Ref. [67].

shows the change of a band gap of GaAs due to the single impurity, which corresponds to an effective concentration of 1.6% in the 128-atom supercell with a TBMBJ [29] potential. Nitrogen is by far the most effective alloying element from the band-gap-reduction point of view, followed by Bi, B, and Sb. The band-gap reduction occurs by either lowering the conduction band or shifting up the valence-band edge, depending on which band edge is primarily affected by the disorder [Fig. 3(b)]. It is the conduction band for N and B and, conversely, the valence band for Bi and Tl (see Table III). These general results are consistent with known trends for dilute nitrides [10] and bismides [68]. This information is relevant for the band-gap engineering in semiconductor heterostructures, where the quantum carrier confinement is a design parameter.

The practical implementation of compound semiconductor alloys is associated with challenges related to their formability. Growth of metastable alloys is a complex process that is largely driven by kinetic effects at the surface, rather than by thermodynamic potentials of the bulk material. A notable example is the incorporation of Bi or N in GaAs that is possible to achieve experimentally at a

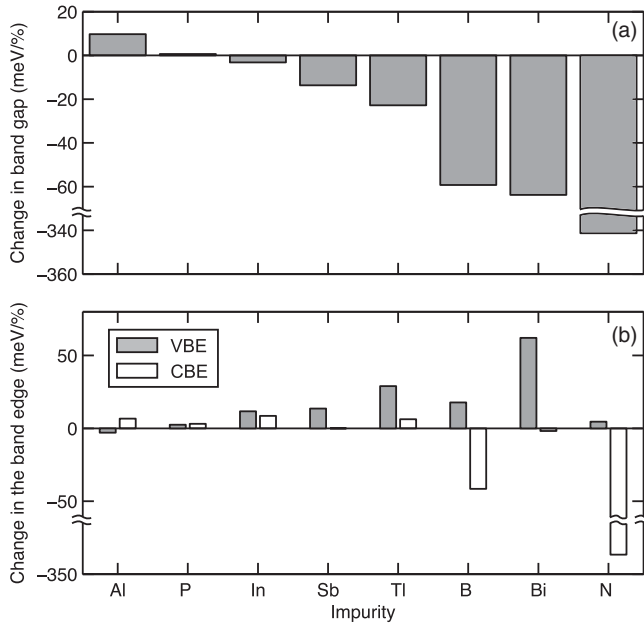


FIG. 3. Effect of single impurities on (a) the band gap and (b) the relative alignment of the band edges in GaAs.

level which exceeds their predicted solubility by several orders of magnitude [69,70]. Although the defect formation enthalpy presented in Fig. 4 cannot be directly related to the solubility, it can still serve as a guideline for evaluating formability of the alloys. Based on these data, one would expect the growth of dilute borides to pose more challenges than thallides or bismides. The energy penalty associated with incorporation of nitrogen in GaAs is at an intermediate level among other group-III-V elements. These results can be understood as an interplay between the chemical bond

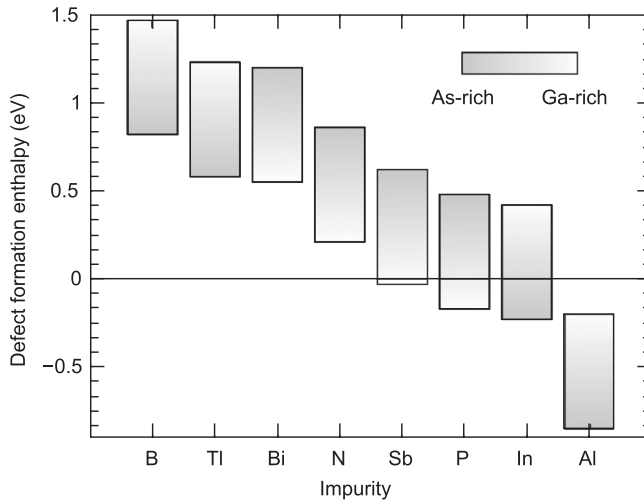


FIG. 4. Formation enthalpy of isovalent substitutional defects in a GaAs host lattice. The lower the enthalpy, the more preferred the impurity is in the host system. The range of energies is linked to the growth conditions that are encoded in the gradient fill.

and local strain energies. The formation enthalpy of BAs is  $-0.31$  eV [71] per formula unit, compared to  $-1.62$  eV [72] for GaN. As a result, the strain energy due to the size mismatch between N and As is partly compensated for by the strong Ga—N bond, which is not the case for the B—As bond. The incorporation of Tl and Bi in GaAs is hindered for the same reason. It is instructive to note that the energy penalty associated with incorporation of a group-III-V element in GaAs (Fig. 4) is not always leveraged through the efficient band-gap reduction or the effective quantum-confinement engineering for semiconducting heterostructures (Fig. 3).

## B. Semiconductor alloys for telecommunication lasers

### 1. $\text{In}_{0.53}\text{Ga}_{0.47}\text{As}$

Extending the preceding impurity study to alloys, we show the link between localization characteristics, the band structure, and properties of gain materials for telecommunication lasers with an emission wavelength of  $1.55 \mu\text{m}$ . We begin with the  $\text{In}_{0.53}\text{Ga}_{0.47}\text{As}$  alloy, which represents the first generation of gain materials. The effective band structure is shown in Fig. 5(a). The calculated band gap of  $0.79$  eV agrees well with the targeted emission wavelength. The Bloch character is well preserved in the vicinity of the band edges and persists approximately  $0.5$  eV into the bands. The light and heavy hole bands, as well as the split-off band, are clearly resolved on the unfolded band structure. The conduction band at the  $L$  valley is energetically well isolated from the  $\Gamma$  valley that prevents spurious interactions and mixing between these states in the alloy.

The above-noted features of the effective alloy band structure are consistent with the narrow low-temperature PL linewidth ( $2\text{--}4$  meV, Ref. [56]), the high mobility of electrons ( $20\,000\text{--}80\,000$   $\text{cm}^2 \text{V}^{-1} \text{s}^{-1}$ , Refs. [56,73]) and holes ( $600\text{--}1000$   $\text{cm}^2 \text{V}^{-1} \text{s}^{-1}$ , Refs. [74,75]) observed experimentally in  $\text{In}_x\text{Ga}_{1-x}\text{As}$ , with  $x \approx 0.5$ . A very narrow ( $0.34$  meV) intrinsic broadening of the band-edge alloy state in the  $\text{In}_{0.5}\text{Ga}_{0.5}\text{P}$  alloy are predicted based on empirical potential calculations [76]. The low value of the localization ratio ( $\zeta < 1$ ) for GaAs:In impurities is consistent with these observations. Therefore,  $\text{In}_{0.53}\text{Ga}_{0.47}\text{As}$  can be viewed as a nearly disorder-free alloy.

The density of states and the IPR spectrum for the  $\text{In}_{0.53}\text{Ga}_{0.47}\text{As}$  alloy are plotted in Fig. 6(a). The magnitude of IPR at the band edges is very close to its disorder-free limit of  $\chi = 1/64$ , which corresponds to the 128-atom supercell. States with a higher excess kinetic energy in the valence and conduction bands show a slight increase of the IPR, particularly in the conduction band when the energy approaches the  $L$  valley ( $E \approx 1.4$  eV). These states do not contribute to inhomogeneous broadening of the optical gain and do not hamper the charge-carrier transport coefficients. However, states with the kinetic energy  $E_k \approx E_g$  are involved in the Auger recombination, which is an important

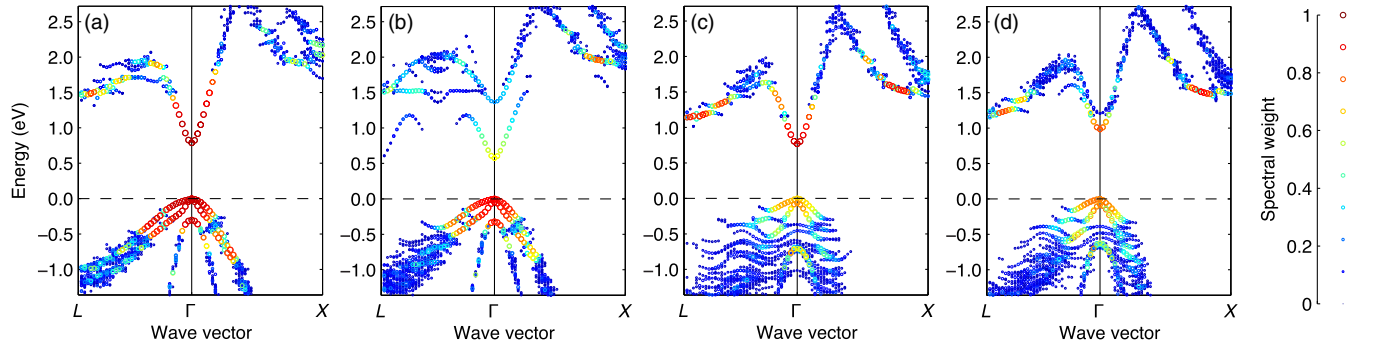


FIG. 5. Effective band structure of semiconductor alloys for telecommunication lasers with an emission wavelength of  $1.55 \mu\text{m}$ . (a)  $\text{In}_{0.53}\text{Ga}_{0.47}\text{As}$ . (b)  $\text{In}_{0.41}\text{Ga}_{0.59}\text{N}_{0.03}\text{As}_{0.94}\text{Sb}_{0.03}$ . (c)  $\text{GaAs}_{0.89}\text{Bi}_{0.11}$ . (d)  $\text{Ga}_{0.91}\text{B}_{0.09}\text{As}_{0.89}\text{Bi}_{0.11}$ . The origin of the energy scale is set at the Fermi energy. The legend on the right shows the Bloch spectral weight. Only data points with a spectral weight of 5% of greater are shown.

loss mechanism for lasers. Implications of the disorder for the Auger recombination are discussed below.

## 2. $\text{In}_{0.41}\text{Ga}_{0.59}\text{N}_{0.03}\text{As}_{0.94}\text{Sb}_{0.03}$

Dilute nitride semiconductors represent the second generation of gain materials designed for an emission wavelength of  $1.55 \mu\text{m}$  and a monolithic integration on a GaAs substrate [77]. The effective band structure of  $\text{In}_{0.41}\text{Ga}_{0.59}\text{N}_{0.03}\text{As}_{0.94}\text{Sb}_{0.03}$  is illustrated in Fig. 5(b). The enhanced statistics of In—N bonds is incorporated into the atomistic structure to model the effect of annealing on material characteristics. The Bloch character in the valence band structure remains well defined similar to (In,Ga)As, which corresponds with a similar IPR spectrum [Figs. 6(b)]. The CBE has drastically changed from (In,Ga)As. The retention of its  $\Gamma$  character is only about 50% [Fig. 5(b)], which is accompanied by the abrupt increase of the IPR (i.e., localization) within the conduction band and near the edge [Fig. 6(b)]. It is worth noting that the strength of localization in the conduction band *increases* with increasing the electron excess energy, contrary to the common view based on the classical Anderson model of localization. The largest IPR value of nearly 0.06 can be interpreted as an orbital wave function being localized in the vicinity of  $0.06^{-1} \approx 17$  atoms only. This observation is consistent with the low Bloch character (less than 30%) for states within the energy window  $E = 1.0\text{--}1.3 \text{ eV}$  [Fig. 5(b)].

These features of the electronic structure of dilute nitrides lead to a broadening of the PL linewidth (18–40 meV, Refs. [8,77–79]) and a reduction of the electron mobility ( $100 \text{ cm}^2 \text{ V}^{-1} \text{ s}^{-1}$ , Ref. [80]), whereas the hole mobility remains unaffected ( $900 \text{ cm}^2 \text{ V}^{-1} \text{ s}^{-1}$ , Ref. [80]). These observations also conform with the single-impurity (GaAs:N and GaAs:Sb) localization studies presented in the preceding subsection. One can anticipate a detrimental impact of localization at the CBE on the optical gain in this material system. The reason for an intrinsic “disorder penalty” is twofold: (i) smearing of the Bloch

character impedes the  $k$ -selection rules for the optical transition and reduces the dipole matrix element, and (ii) the inhomogeneous broadening reduces the gain.

## 3. $\text{GaAs}_{0.89}\text{Bi}_{0.11}$

We now turn to the third generation of the gain materials, namely, dilute bismide  $\text{GaAs}_{1-x}\text{Bi}_x$  alloys. Their development is inspired by a potential ability to reduce the Auger losses [81]. The bismuth content of  $x = 0.11$  is selected to match an anticipated band gap with an emission wavelength of  $1.55 \mu\text{m}$  [13]. The band structure of  $\text{GaAs}_{0.89}\text{Bi}_{0.11}$  is shown in Fig. 5(c). Contrary to the dilute nitrides, the bismides demonstrate a well-defined profile in the conduction band, whereas the valence band is severely distorted [20,32]. The conduction-band minimum is well resolved, with a strong  $\Gamma$  character without a noticeable mixing with  $L$  and  $X$  states. The split-off band is located at  $\Delta_{\text{SO}} = 0.72 \text{ eV}$  below the valence-band edge. At such a high bismuth content, the spin-orbit splitting approaches the band gap, which is  $E_g = 0.77 \text{ eV}$  in our case ( $\Delta_{\text{SO}} > E_g$  is desired for a suppression of the Auger recombination). In both material systems, (In,Ga)As and (Ga,In)(N,As,Sb), which are studied above, this condition is far from being fulfilled.

Examining the localization effects in  $\text{GaAs}_{0.89}\text{Bi}_{0.11}$  [Fig. 6(c)], we discern that states at the valence-band edge have a degree of localization comparable to (Ga,In)(N,As,Sb) alloys. These results explain the broad low-temperature PL linewidth of Ga(As,Bi) alloys (60–70 meV, Refs. [82,83]) and the steep decline of the hole mobility ( $6\text{--}15 \text{ cm}^2 \text{ V}^{-1} \text{ s}^{-1}$ , Refs. [67,84]). Dilute bismides exhibit stronger localization effects than dilute nitrides, even though the localization in GaAs:Bi is less pronounced at the single-impurity level than in GaAs:N ( $\zeta_{\text{Bi}}^{\text{VBE}} < \zeta_{\text{N}}^{\text{CBE}}$ ; see Table III). The enhanced localization in dilute bismides can be attributed to the much higher concentration of bismuth, which is required to achieve the same band-gap reduction as in dilute nitrides. Accordingly, the alloy statistics leads to

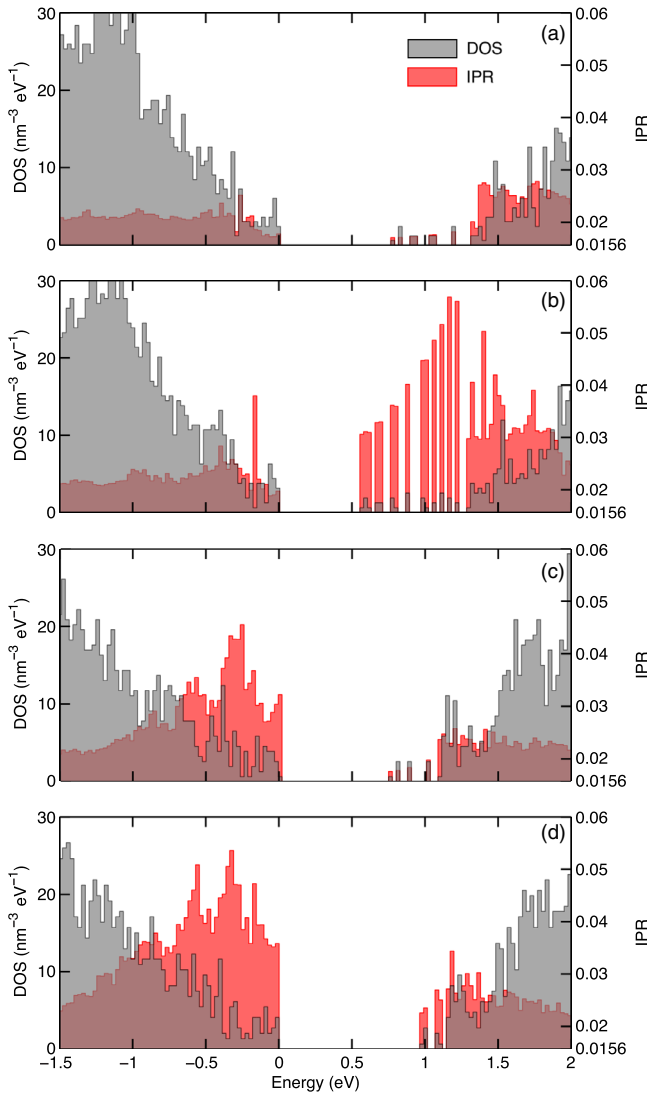


FIG. 6. Density of states (DOS) shown alongside the inverse participation ratio (IPR), which captures the strength of localization in semiconductor alloys for telecommunication lasers with the emission wavelength of  $1.55 \mu\text{m}$ . (a)  $\text{In}_{0.53}\text{Ga}_{0.47}\text{As}$ . (b)  $\text{In}_{0.41}\text{Ga}_{0.59}\text{N}_{0.03}\text{As}_{0.94}\text{Sb}_{0.03}$ . (c)  $\text{GaAs}_{0.89}\text{Bi}_{0.11}$ . (d)  $\text{Ga}_{0.91}\text{B}_{0.09}\text{As}_{0.89}\text{Bi}_{0.11}$ . The lower limit of IPR  $1/64$  corresponds to pure Bloch states in the 128-atom supercell.

a higher probability of forming pairs (Bi-Ga-Bi) and higher-order clusters, which have a detrimental effect on the electronic structure at the VBE [20,48].

The above discussion of the disorder penalty and its impact on gain characteristics is fully applicable to the Ga(As,Bi) material system. The disorder also has implications on optical losses. The Auger recombination is a many-particle process, the likelihood of which is determined by the energy and momentum (wave-vector) conservation of the electronic states involved. In materials with strong disorder, the momentum-conservation requirement is relaxed due to uncertainties of the wave vector  $\mathbf{k}$  inherent to localized states. Therefore, the inferred reduction of

Auger losses in Ga(As,Bi) gain media requires a thorough analysis, which will take into account the realistic band structure shown in Fig. 5(c) and the presence of alloy disorder.

#### 4. $\text{Ga}_{0.91}\text{B}_{0.09}\text{As}_{0.89}\text{Bi}_{0.11}$

Finally, we would like to comment on quaternary bismide alloys. For instance, the Ga(N,As,Bi) material system [81,85] offers an additional flexibility in engineering of the lattice mismatch and/or band offsets. Here, we study a  $\text{Ga}_{0.91}\text{B}_{0.09}\text{As}_{0.89}\text{Bi}_{0.11}$  alloy, which is inspired by the physics of In—N bonds in (Ga,In)(N,As) [18,86]. One would expect that the incorporation of boron will further reduce the band gap and help to mitigate the local strain fields by forming B—Bi bonds (a correlated alloy). By contrast, the addition of boron results in an upward shift of the  $\Gamma$  valley of the conduction band and an opening of the band gap [Fig. 5(d)]. This result suggests that the properties of quaternary alloys are governed by more-complicated physics than a simple additive effects of ternary compounds. The positive effect of boron is an improvement of the Bloch character of the VBE [Fig. 5(d)] compared to the boron-free alloy [Fig. 5(c)]. However, there are two drawbacks: (i) a more-severe localization develops in the conduction band and deeper energy states in the valence band, and (ii) the incorporation of boron in a GaAs lattice can be challenging due to the high defect formation energy (Fig. 4). Nevertheless, (Ga,B)(As,Bi) could be an alternative material system for multijunction solar cells with a 1-eV band gap and lattice matched to GaAs.

It is important to note that the results presented above are obtained for bulk materials, which does not take into account an epitaxial strain that can arise from a lattice mismatch between the layer and the substrate. The strain is not an issue for  $\text{In}_{0.53}\text{Ga}_{0.47}\text{As}$  and  $\text{Ga}_{0.91}\text{B}_{0.09}\text{As}_{0.89}\text{Bi}_{0.11}$  alloys, as their lattice constant is intended to match the substrates, InP and GaAs, respectively. By contrast,  $\text{In}_{0.41}\text{Ga}_{0.59}\text{N}_{0.03}\text{As}_{0.94}\text{Sb}_{0.03}$  and  $\text{GaAs}_{0.89}\text{Bi}_{0.11}$  alloys possess a lattice mismatch of 2.6% and 1.4% with respect to GaAs (see the theoretical lattice parameters in Tables I and II). Two methods, namely, Matthews and Blakeslee [87] and Voisin [88], are used to assess a critical thickness  $h_c$  of the film that can accommodate the epitaxial strain elastically without generating misfit dislocations. Both approaches produce similar results of  $h_c = 2.5 \text{ nm}$  for  $\text{In}_{0.41}\text{Ga}_{0.59}\text{N}_{0.03}\text{As}_{0.94}\text{Sb}_{0.03}/\text{GaAs}$  and  $6 \text{ nm}$  for  $\text{GaAs}_{0.89}\text{Bi}_{0.11}/\text{GaAs}$  heterostructures. Layers with a thickness less than  $h_c$  will be tetragonally distorted, which may have an additional impact on localization characteristics. We evaluate the effect of a tetragonal distortion on the electronic structure and localization in the compressively strained  $\text{GaAs}_{0.89}\text{Bi}_{0.11}$  compound on a GaAs substrate (see the Appendix). The tetragonal distortion leads to an opening of the band gap and a lifting of the degeneracy between heavy and light holes, which is consistent with effects

expected from a compressive in-plane strain of the layer [88]. There are no major changes observed in the IPR spectrum, indicating that the alloy disorder is not sensitive to the epitaxial strain for the particular material system and the strain magnitude.

#### IV. CONCLUSIONS

DFT calculations are used to perform a systematic characterization of isovalent impurities (B, N, Al, P, In, Sb, Tl, and Bi) in the host GaAs. The degree of localization present in electronic states near the band edges decreases in the following order: N, Bi, B, Tl, and Sb. Other elements do not cause a notable localization of the electronic states. The localization strength scales with the Born effective charge, which is calculated for individual impurities. The effective charge of impurities can be markedly different from their nominal values in binary compounds reflecting their electropositive or electronegative nature in the specific host lattice. Elements which have a Born effective charge less than the host introduce localized states in the conduction band but do not perturb the valence-band edge, and vice versa. The extremity of localization at the band edges directly correlates with several important characteristics, such as the charge-carrier transport, broadening of the photoluminescence spectra, the ability of individual elements to change the band gap, and the relative band alignment. An extensive comparison with experimental data gives confidence in the predictive power of first-principles calculations. The energy penalty associated with incorporation of impurities in the host lattice does not follow the localization pattern and decreases in the following order: B, Tl, Bi, N, and Sb. This result implies that the growth of dilute borides poses more challenges than thallides or bismides. The incorporation of nitrogen in GaAs is assisted by the strong Ga—N bond.

We perform a comparative study of localization in (In,Ga)As, (Ga,In)(N,As,Sb) and Ga(As,Bi) compound alloys, which represent three generations of material systems for telecommunication lasers. A wave-function inverse participation ratio calculated for individual eigenstates is used as a measure for the extremity of localization. The results indicate that the electronic structure of (In,Ga)As is least affected by the alloy disorder. The electronic states near the conduction-band edge of (Ga,In)(N,As,Sb) and the valence-band edges of Ga(As,Bi) are strongly affected by the disorder. The extremity of localization at the valence-band edge of Ga(As,Bi) is approximately 2 times greater than that for the conduction-band edge of (Ga,In)(N,As,Sb). This result translates into an intrinsically higher inhomogeneous broadening inherent to dilute bismide alloys compared to their dilute nitride counterparts, which can have an unfavorable impact on the optical gain characteristics and Auger losses. This conclusion should not be extended to group-III antimonide semiconductors alloyed with Bi for midinfrared devices. The smaller

electronic difference between Sb and Bi should lead to a less detrimental impact of Bi on the structure of (Al,Ga,In)(Sb,Bi), according to the arguments presented above for single impurities.

#### ACKNOWLEDGMENTS

The authors are thankful to Axel van de Walle and Joseph Zwanziger for the helpful discussions regarding the generation of quasirandom structures, as well as to Maciej Polak for the critical reading of the manuscript. Funding is provided by the Natural Sciences and Engineering Research Council of Canada under Discovery Grant Program No. RGPIN-2015-04518. This work was performed using computational resources of the Thunder Bay Regional Research Institute, Lakehead University, and Compute Canada (Calcul Quebec).

#### APPENDIX: EFFECT OF THE EPITAXIAL STRAIN (TETRAGONAL DISTORTION)

The effect of epitaxial strain on the electronic structure of  $\text{GaAs}_{0.89}\text{Bi}_{0.11}$  is studied using a 128-atom supercell. The lattice parameters in lateral directions ( $a_c$  and  $b_c$ ) are fixed to that of GaAs [Fig. 7(a)]; the  $c_c$  lattice constant remains unconstrained. The lattice parameters and angles of the rhombohedral primitive cell are scaled to reproduce the tetragonal lattice distortion, as shown in Fig. 7(a).

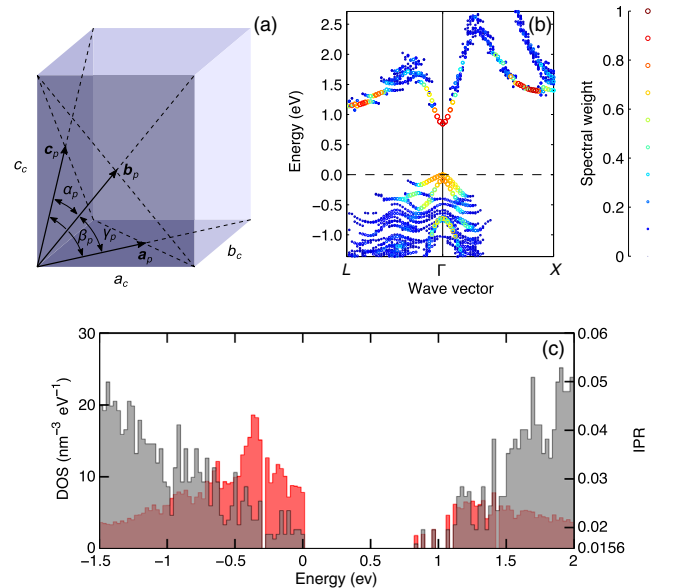


FIG. 7. Effect of epitaxial strain on the electronic structure of  $\text{GaAs}_{0.89}\text{Bi}_{0.11}$ . (a) Conventional unit cell with a tetragonal distortion in relation to the primitive lattice vectors  $\mathbf{a}_p$ ,  $\mathbf{b}_p$ , and  $\mathbf{c}_p$ , and angles. (b) Unfolded band structure. The wave vectors are selected within the growth plane (001). (c) Density of states (DOS) and the inverse participation ratio (IPR). The origin of the energy scale is set at the Fermi energy.

The most noticeable changes in the electronic structure of  $\text{GaAs}_{0.89}\text{Bi}_{0.11}$  due to the epitaxial strain are an opening of the band gap by approximately 0.1 eV and a lifting up of the degeneracy at the top of the valence band [Fig. 7(b)]. The Bloch character, the density of states, and localization characteristics assessed via the inverse participation ratio do not show any prominent changes compared to the bulk material [Figs. 5(c) and 6(c)].

- 
- [1] Masafumi Yamaguchi, Tatsuya Takamoto, Kenji Araki, and Nicholas Ekins-Daukes, Multi-junction III–V solar cells: Current status and future potential, *Solar Energy* **79**, 78 (2005).
- [2] Chaturvedi Gogineni, Nathaniel A. Riordan, Shane R. Johnson, Xianfeng Lu, and Tom Tiedje, Disorder and the Urbach edge in dilute bismide GaAsBi, *Appl. Phys. Lett.* **103**, 041110 (2013).
- [3] Igor P. Marko, Christopher A. Broderick, Shirong Jin, Peter Ludewig, Wolfgang Stolz, Kerstin Volz, Judy M. Rorison, Eoin P. O’Reilly, and Stephen J. Sweeney, Optical gain in GaAsBi/GaAs quantum well diode lasers, *Sci. Rep.* **6**, 28863 (2016).
- [4] C. A. Broderick, M. Usman, S. J. Sweeney, and E. P. O’Reilly, Band engineering in dilute nitride and bismide semiconductor lasers, *Semicond. Sci. Technol.* **27**, 094011 (2012).
- [5] Masahiko Kondow, Kazuhisa Uomi, Atsuko Niwa, Takeshi Kitatani, Seiji Watahiki, and Yoshiaki Yazawa, GaInNAs: A novel material for long-wavelength-range laser diodes with excellent high-temperature performance, *Jpn. J. Appl. Phys.* **35**, 1273 (1996).
- [6] M. Kneissl, T. Kolbe, C. Chua, V. Kueller, N. Lobo, J. Stellmach, A. Knauer, H. Rodriguez, S. Einfeldt, Z. Yang, N. M. Johnson, and M. Weyers, Advances in group III-nitride-based deep UV light-emitting diode technology, *Semicond. Sci. Technol.* **26**, 014036 (2011).
- [7] K. Alberi, J. Wu, W. Walukiewicz, K. M. Yu, O. D. Dubon, S. P. Watkins, C. X. Wang, X. Liu, Y.-J. Cho, and J. Furdyna, Valence-band anticrossing in mismatched III–V semiconductor alloys, *Phys. Rev. B* **75**, 045203 (2007).
- [8] O. Rubel, M. Galluppi, S. D. Baranovskii, K. Volz, L. Geelhaar, H. Riechert, P. Thomas, and W. Stolz, Quantitative description of disorder parameters in (GaIn)(NAs) quantum wells from the temperature-dependent photoluminescence spectroscopy, *J. Appl. Phys.* **98**, 063518 (2005).
- [9] T. Tiedje, E. C. Young, and A. Mascarenhas, Growth and properties of the dilute bismide semiconductor  $\text{GaAs}_{1-x}\text{Bi}_x$  a complementary alloy to the dilute nitrides, *Int. J. Nanotechnology* **5**, 963 (2008).
- [10] P. R. C. Kent and A. Zunger, Theory of electronic structure evolution in GaAsN and GaPN alloys, *Phys. Rev. B* **64**, 115208 (2001).
- [11] Yong Zhang, A. Mascarenhas, and L.-W. Wang, Similar and dissimilar aspects of III–V semiconductors containing Bi versus N, *Phys. Rev. B* **71**, 155201 (2005).
- [12] Yong Zhang, A. Mascarenhas, and L.-W. Wang, Systematic approach to distinguishing a perturbed host state from an impurity state in a supercell calculation for a doped semiconductor: Using GaP:N as an example, *Phys. Rev. B* **74**, 041201 (2006).
- [13] A. R. Mohmad, F. Bastiman, C. J. Hunter, R. D. Richards, S. J. Sweeney, J. S. Ng, J. P. R. David, and B. Y. Majlis, Localization effects and band gap of GaAsBi alloys, *Phys. Status Solidi B* **251**, 1276 (2014).
- [14] Weng W. Chow and Stephan W. Koch, *Semiconductor-Laser Fundamentals: Physics of the Gain Materials* (Springer Science+Business Media, New York, 1999).
- [15] E. Fred Schubert and Jong Kyu Kim, Solid-state light sources getting smart, *Science* **308**, 1274 (2005).
- [16] S. V. Dudiy and Alex Zunger, Searching for Alloy Configurations with Target Physical Properties: Impurity Design via a Genetic Algorithm Inverse Band Structure Approach, *Phys. Rev. Lett.* **97**, 046401 (2006).
- [17] L. Bellaiche, S. H. Wei, and Alex Zunger, Localization and percolation in semiconductor alloys: GaAsN vs GaAsP, *Phys. Rev. B* **54**, 17568 (1996).
- [18] P. J. Klar, H. Grüning, J. Koch, S. Schäfer, K. Volz, W. Stolz, W. Heimbrod, A. M. Kamal Saadi, A. Lindsay, and E. P. O’Reilly, (Ga,In)(N,As)-fine structure of the band gap due to nearest-neighbor configurations of the isovalent nitrogen, *Phys. Rev. B* **64**, 121203(R) (2001).
- [19] Muhammad Usman, Christopher A. Broderick, Zahida Batool, Konstanze Hild, Thomas J. C. Hosea, Stephen J. Sweeney, and Eoin P. O’Reilly, Impact of alloy disorder on the band structure of compressively strained  $\text{GaBi}_x\text{As}_{1-x}$ , *Phys. Rev. B* **87**, 115104 (2013).
- [20] Lars C. Bannow, Oleg Rubel, Stefan C. Badescu, Phil Rosenow, Jörg Hader, Jerome V. Moloney, Ralf Tonner, and Stephan W. Koch, Configuration dependence of band-gap narrowing and localization in dilute  $\text{GaAs}_{1-x}\text{Bi}_x$  alloys, *Phys. Rev. B* **93**, 205202 (2016).
- [21] Hui-Xiong Deng, Jingbo Li, Shu-Shen Li, Haowei Peng, Jian-Bai Xia, Lin-Wang Wang, and Su-Huai Wei, Band crossing in isovalent semiconductor alloys with large size mismatch: First-principles calculations of the electronic structure of Bi and N incorporated GaAs, *Phys. Rev. B* **82**, 193204 (2010).
- [22] P. W. Anderson, Absence of diffusion in certain random lattices, *Phys. Rev.* **109**, 1492 (1958).
- [23] Franz Wegner, Inverse participation ratio in  $2 + \epsilon$  dimensions, *Z. Phys. B* **36**, 209 (1980).
- [24] Bernhard Kramer and Angus MacKinnon, Localization: Theory and experiment, *Rep. Prog. Phys.* **56**, 1469 (1993).
- [25] W. Kohn and L. J. Sham, Self-consistent equations including exchange and correlation effects, *Phys. Rev.* **140**, A1133 (1965).
- [26] P. Blaha, K. Schwarz, G. K. H. Madsen, D. Kvasnicka, and J. Luitz, *WIEN2K: An Augmented Plane Wave+Local Orbitals Program for Calculating Crystal Properties* (Technische Universität Wien, Austria, 2001).
- [27] H. J. Monkhorst and J. D. Pack, Special points for Brillouin-zone integrations, *Phys. Rev. B* **13**, 5188 (1976).
- [28] Zhigang Wu and R. E. Cohen, More accurate generalized gradient approximation for solids, *Phys. Rev. B* **73**, 235116 (2006).
- [29] Fabien Tran and Peter Blaha, Accurate Band Gaps of Semiconductors and Insulators with a Semilocal

- Exchange-Correlation Potential, *Phys. Rev. Lett.* **102**, 226401 (2009).
- [30] I. Vurgaftman, J. R. Meyer, and L. R. Ram-Mohan, Band parameters for III-V compound semiconductors and their alloys, *J. Appl. Phys.* **89**, 5815 (2001).
- [31] I. Vurgaftman and J. R. Meyer, Band parameters for nitrogen-containing semiconductors, *J. Appl. Phys.* **94**, 3675 (2003).
- [32] O. Rubel, A. Bokhanchuk, S. J. Ahmed, and E. Assmann, Unfolding the band structure of disordered solids: From bound states to high-mobility Kane fermions, *Phys. Rev. B* **90**, 115202 (2014).
- [33] S. J. Ahmed, J. Kivinen, B. Zaporzan, L. Curiel, S. Pichardo, and O. Rubel, BERRYPI: A software for studying polarization of crystalline solids with WIEN2K density functional all-electron package, *Comput. Phys. Commun.* **184**, 647 (2013).
- [34] N. C. Murphy, R. Wortis, and W. A. Atkinson, Generalized inverse participation ratio as a possible measure of localization for interacting systems, *Phys. Rev. B* **83**, 184206 (2011).
- [35] Christoph Freysoldt, Blazej Grabowski, Tilmann Hickel, Jörg Neugebauer, Georg Kresse, Anderson Janotti, and Chris G. Van de Walle, First-principles calculations for point defects in solids, *Rev. Mod. Phys.* **86**, 253 (2014).
- [36] Georg Kresse and Jürgen Furthmüller, Efficient iterative schemes for *ab initio* total-energy calculations using a plane-wave basis set, *Phys. Rev. B* **54**, 11169 (1996).
- [37] G. Kresse and D. Joubert, From ultrasoft pseudopotentials to the projector augmented-wave method, *Phys. Rev. B* **59**, 1758 (1999).
- [38] P. E. Blöchl, Projector augmented-wave method, *Phys. Rev. B* **50**, 17953 (1994).
- [39] John P. Perdew, Kieron Burke, and Matthias Ernzerhof, Generalized Gradient Approximation Made Simple, *Phys. Rev. Lett.* **77**, 3865 (1996).
- [40] Mohamed Tmar, Armand Gabriel, Christian Chatillon, and Ibrahim Ansara, Critical analysis and optimization of the thermodynamic properties and phase diagrams of the III-V compounds II. The Ga-As and In-As systems, *J. Cryst. Growth* **69**, 421 (1984).
- [41] Geoffroy Hautier, Shyue Ping Ong, Anubhav Jain, Charles J. Moore, and Gerbrand Ceder, Accuracy of density functional theory in predicting formation energies of ternary oxides from binary oxides and its implication on phase stability, *Phys. Rev. B* **85**, 155208 (2012).
- [42] Alex Zunger, S.-H. Wei, L. G. Ferreira, and James E. Bernard, Special Quasirandom Structures, *Phys. Rev. Lett.* **65**, 353 (1990).
- [43] A. Van de Walle, P. Tiwary, M. De Jong, D. L. Olmsted, M. Asta, A. Dick, D. Shin, Y. Wang, L.-Q. Chen, and Z.-K. Liu, Efficient stochastic generation of special quasirandom structures, *CALPHAD: Comput. Coupling Phase Diagrams Thermochem.* **42**, 13 (2013).
- [44] A. L. Allred, Electronegativity values from thermochemical data, *J. Inorg. Nucl. Chem.* **17**, 215 (1961).
- [45] A. R. Goñi, H. Siegle, K. Syassen, C. Thomsen, and J.-M. Wagner, Effect of pressure on optical phonon modes and transverse effective charges in GaN and AlN, *Phys. Rev. B* **64**, 035205 (2001).
- [46] W. A. Harrison, *Electronic Structure and Properties of Solids* (Dover, New York, 1989).
- [47] A. Lindsay and E. P. O'Reilly, Unification of the Band Anticrossing and Cluster-State Models of Dilute Nitride Semiconductor Alloys, *Phys. Rev. Lett.* **93**, 196402 (2004).
- [48] Muhammad Usman, Christopher A. Broderick, Andrew Lindsay, and Eoin P. O'Reilly, Tight-binding analysis of the electronic structure of dilute bismide alloys of GaP and GaAs, *Phys. Rev. B* **84**, 245202 (2011).
- [49] E. Hal Bogardus and H. Barry Bebb, Bound-exciton, free-exciton, band-acceptor, donor-acceptor, and Auger recombination in GaAs, *Phys. Rev.* **176**, 993 (1968).
- [50] J. D. Wiley, in *Semiconductors and Semimetals*, Vol. 10, edited by R. K. Willardson and Albert Beer (Academic Press, New York, 1975), p. 91.
- [51] G. E. Stillman, C. M. Wolfe, and J. O. Dimmock, Hall coefficient factor for polar mode scattering in *n*-type GaAs, *J. Phys. Chem. Solids* **31**, 1199 (1970).
- [52] V. Gottschalch, G. Leibiger, and G. Benndorf, MOVPE growth of  $B_xGa_{1-x}As$ ,  $B_xGa_{1-x-y}In_yAs$ , and  $B_xAl_{1-x}As$  alloys on (001) GaAs, *J. Cryst. Growth* **248**, 468 (2003).
- [53] R. Hamila, F. Saidi, P. H. Rodriguez, Laurent Auvray, Y. Monteil, and H. Maaref, Growth temperature effects on boron incorporation and optical properties of BGaAs/GaAs grown by MOCVD, *J. Alloys Compd.* **506**, 10 (2010).
- [54] D. C. Reynolds, K. K. Bajaj, C. W. Litton, P. W. Yu, Jasprit Singh, W. T. Masselink, R. Fischer, and H. Morkoç, Determination of interfacial quality of GaAs-GaAlAs multi-quantum well structures using photoluminescence spectroscopy, *Appl. Phys. Lett.* **46**, 51 (1985).
- [55] Michael Shur, *Physics of Semiconductor Devices* (Prentice-Hall, Englewood Cliffs, NJ, 1990).
- [56] H. Protzmann, F. Höhnsdorf, Z. Spika, W. Stolz, E. O. Göbel, M. Müller, and J. Lorberth, Properties of  $(Ga_{0.47}In_{0.53})As$  epitaxial layers grown by metalorganic vapor phase epitaxy (MOVPE) using alternative arsenic precursors, *J. Cryst. Growth* **170**, 155 (1997).
- [57] W. C. Mitchel and P. W. Yu, Study of electronic levels in antimony and indium-doped gallium arsenide, *J. Appl. Phys.* **57**, 623 (1985).
- [58] Otfried Madelung and Sadao Adachi, *Landolt-Börnstein: Numerical Data and Functional Relationships in Science and Technology* (Springer, New York, 2002).
- [59] R. Kudrawiec, M. Latkowska, M. Baranowski, J. Misiewicz, L. H. Li, and J. C. Harmand, Photorefectance, photoluminescence, and microphotoluminescence study of optical transitions between delocalized and localized states in  $GaN_{0.02}As_{0.98}$ ,  $Ga_{0.95}In_{0.05}N_{0.02}As_{0.98}$ , and  $GaN_{0.02}As_{0.90}Sb_{0.08}$  layers, *Phys. Rev. B* **88**, 125201 (2013).
- [60] J. Plaza, J. L. Castaño, B. J. García, H. Carrère, and E. Bedel-Pereira, Temperature dependence of photoluminescence and photorefectance spectra of dilute GaAsN alloys, *Appl. Phys. Lett.* **86**, 121918 (2005).
- [61] S. Dhar, A. Mondal, and T. D. Das, Hall mobility and electron trap density in GaAsN grown by liquid phase epitaxy, *Semicond. Sci. Technol.* **23**, 015007 (2008).
- [62] James J. Tietjen and James A. Amick, The preparation and properties of vapor-deposited epitaxial  $GaAs_{1-x}P_x$  using arsine and phosphine, *J. Electrochem. Soc.* **113**, 724 (1966).

- [63] D. Huang, J. Chyi, J. Klem, and Hadis Morkoc, Optical properties of molecular beam epitaxially grown  $\text{GaAs}_{1-x}\text{Sb}_x$  ( $0 < x < 0.5$ ) on GaAs and InP substrates, *J. Appl. Phys.* **63**, 5859 (1988).
- [64] C. R. Bolognesi, M. M. W. Dvorak, P. Yeo, X. G. Xu, and S. P. Watkins, InP/GaAsSb/InP double HBTs: A new alternative for InP-based DHBTs, *IEEE Trans. Electron Devices* **48**, 2631 (2001).
- [65] Kunishige Oe, Characteristics of semiconductor alloy  $\text{GaAs}_{1-x}\text{Bi}_x$ , *Jpn. J. Appl. Phys.* **41**, 2801 (2002).
- [66] S. Francoeur, S. Tixier, E. Young, T. Tiedje, and A. Mascarenhas, Bi isoelectronic impurities in GaAs, *Phys. Rev. B* **77**, 085209 (2008).
- [67] R. N. Kini, A. J. Ptak, B. Fluegel, R. France, R. C. Reedy, and A. Mascarenhas, Effect of Bi alloying on the hole transport in the dilute bismide alloy  $\text{GaAs}_{1-x}\text{Bi}_x$ , *Phys. Rev. B* **83**, 075307 (2011).
- [68] M. P. Polak, P. Scharoch, and R. Kudrawiec, First-principles calculations of bismuth induced changes in the band structure of dilute Ga-V-Bi and In-V-Bi alloys: Chemical trends versus experimental data, *Semicond. Sci. Technol.* **30**, 094001 (2015).
- [69] S. B. Zhang and Su-Huai Wei, Nitrogen Solubility and Induced Defect Complexes in Epitaxial GaAs:N, *Phys. Rev. Lett.* **86**, 1789 (2001).
- [70] Andreas Beyer, Wolfgang Stolz, and Kerstin Volz, Metastable cubic zinc-blende III/V semiconductors: Growth and structural characteristics, *Prog. Cryst. Growth Charact. Mater.* **61**, 46 (2015).
- [71] H. Dumont and Y. Monteil, Some aspects on thermodynamic properties, phase diagram and alloy formation in the ternary system BAs-GaAs—Part I: Analysis of BAs thermodynamic properties, *J. Cryst. Growth* **290**, 410 (2006).
- [72] M. R. Ranade, F. Tessier, A. Navrotsky, V. J. Leppert, S. H. Risbud, F. J. DiSalvo, and C. M. Balkas, Enthalpy of formation of gallium nitride, *J. Phys. Chem. B* **104**, 4060 (2000).
- [73] Yoshikazu Takeda, Akio Sasaki, Yujiro Imamura, and Toshinori Takagi, Electron mobility and energy gap of  $\text{In}_{0.53}\text{Ga}_{0.47}\text{As}$  on InP substrate, *J. Appl. Phys.* **47**, 5405 (1976).
- [74] M. Sotoodeh, A. H. Khalid, and A. A. Rezazadeh, Empirical low-field mobility model for III–V compounds applicable in device simulation codes, *J. Appl. Phys.* **87**, 2890 (2000).
- [75] P. S. Menon, K. Kandiah, and S. Shaari, Concentration and temperature-dependent low-field mobility model for  $\text{In}_{0.53}\text{Ga}_{0.47}\text{As}$  interdigitated lateral pin PD, *IEICE Electron. Express* **5**, 303 (2008).
- [76] Yong Zhang and Lin-Wang Wang, Global electronic structure of semiconductor alloys through direct large-scale computations for III–V alloys  $\text{Ga}_x\text{In}_{1-x}\text{P}$ , *Phys. Rev. B* **83**, 165208 (2011).
- [77] Seth R. Bank, Hopil Bae, Lynford L. Goddard, Homan B. Yuen, Mark A. Wistey, Robert Kudrawiec, and James S. Harris, Recent progress on 1.55- $\mu\text{m}$  dilute-nitride lasers, *IEEE J. Quantum Electron.* **43**, 773 (2007).
- [78] Seth R. Bank, Mark A. Wistey, Lynford L. Goddard, Homan B. Yuen, Vincenzo Lordi, and James S. Harris, Jr., Low-threshold continuous-wave 1.5- $\mu\text{m}$  GaInNASb lasers grown on GaAs, *IEEE J. Quantum Electron.* **40**, 656 (2004).
- [79] Lynford L. Goddard, Seth R. Bank, Mark A. Wistey, Homan B. Yuen, Zhilong Rao, and James S. Harris, Recombination, gain, band structure, efficiency, and reliability of 1.5- $\mu\text{m}$  GaInNASb/GaAs lasers, *J. Appl. Phys.* **97**, 083101 (2005).
- [80] K. Volz, J. Koch, B. Kunert, and W. Stolz, Doping behaviour of Si, Te, Zn and Mg in lattice-matched (GaIn)(NAS)/GaAs bulk films, *J. Cryst. Growth* **248**, 451 (2003).
- [81] S. J. Sweeney and S. R. Jin, Bismide-nitride alloys: Promising for efficient light emitting devices in the near- and mid-infrared, *J. Appl. Phys.* **113**, 043110 (2013).
- [82] M. K. Shakfa, M. Wiemer, P. Ludewig, K. Jandieri, K. Volz, W. Stolz, S. D. Baranovskii, and M. Koch, Thermal quenching of photoluminescence in Ga(AsBi), *J. Appl. Phys.* **117**, 025709 (2015).
- [83] S. Imhof, A. Thränhardt, A. Chernikov, M. Koch, N. S. Köster, S. Chatterjee, S. W. Koch, X. Lu, S. R. Johnson, D. A. Beaton, T. Tiedje, and O. Rubel, Clustering effects in Ga(AsBi), *Appl. Phys. Lett.* **96**, 131115 (2010).
- [84] S. Nargelas, K. Jarašiūnas, K. Bertulis, and V. Pačebutas, Hole diffusivity in GaAsBi alloys measured by a picosecond transient grating technique, *Appl. Phys. Lett.* **98**, 082115 (2011).
- [85] A. Mascarenhas, Yong Zhang, Jason Verley, and M. J. Seong, Overcoming limitations in semiconductor alloy design, *Superlattices Microstruct.* **29**, 395 (2001).
- [86] K. Kim and A. Zunger, Spatial Correlations in GaInAsN Alloys and Their Effects on Band-Gap Enhancement and Electron Localization, *Phys. Rev. Lett.* **86**, 2609 (2001).
- [87] J. W. Matthews and A. E. Blakeslee, Defects in epitaxial multilayers: I. Misfit dislocations, *J. Cryst. Growth* **27**, 118 (1974).
- [88] Paul Voisin, Heterostructures of lattice mismatched semiconductors: Fundamental aspects and device perspectives, *Proc. SPIE Int. Soc. Opt. Eng.* **0861**, 88 (1988).